Simultaneous X-ray and Far-Ultraviolet Spectra of AGN with ASCA and HUT

Gerard A. Kriss
Department of Physics & Astronomy, Johns Hopkins University, Baltimore, MD 21218

ABSTRACT

We obtained ASCA spectra of the Seyfert 1 galaxy NGC 3516 in March 1995. Simultaneous far-UV observations were obtained with the Hopkins Ultraviolet Telescope on the Astro-2 shuttle mission. The ASCA spectrum shows a lightly absorbed power law of energy index 0.78. The low energy absorbing column is significantly less than previously seen. Prominent O VII and O VIII absorption edges are visible, but, consistent with the much lower total absorbing column, no Fe K absorption edge is detectable. A weak, narrow Fe Kα emission line from cold material is present as well as a broad Fe Kα line. These features are similar to those reported in other Seyfert 1 galaxies. A single warm absorber model provides only an imperfect description of the low energy absorption. In addition to a highly ionized absorber with ionization parameter $U = 1.66$ and a total column density of 1.4×10^{22} cm^{-2}, adding a lower ionization absorber with $U = 0.32$ and a total column of 6.9×10^{21} cm^{-2} significantly improves the fit. The contribution of resonant line scattering to our warm absorber models limits the Doppler parameter to < 160 km s^{-1} at 90% confidence. Turbulence at the sound speed of the photoionized gas provides the best fit. None of the warm absorber models fit to the X-ray spectrum can match the observed equivalent widths of all the UV absorption lines. Accounting for the X-ray and UV absorption simultaneously requires an absorbing region with a broad range of ionization parameters and column densities.

Final technical report submitted to NASA for grant NAG5-2935.

Gerard A. Kriss
Gerard A. Kriss
Principle Investigator
December 8, 1997

1. Introduction

Intrinsic absorption is a valuable tool for probing structures in active galactic nuclei (AGN). While absorption may in principle arise anywhere in the host galaxy, the most interesting absorbers are those that appear to be associated with the central engine. These "warm absorbers" commonly appear in the X-ray spectra of AGN (Turner et al. 1993; Nandra & Pounds 1994), and they could be material in the broad-emission-line region (BELR) (e.g. Netzer 1993; Reynolds & Fabian 1995) or the X-ray heated wind which forms the reflecting region in type 2 AGN (Krolik & Kriss 1995), or an entirely new component. If X-ray warm absorbers are related to associated UV absorption systems (Mathur et al. 1994; Mathur, Wilkes, & Elvis 1995), then UV and X-ray observations together place powerful constraints on the ionization structure of the absorber. In the X-ray one can measure the column densities of highly ionized species (e.g. O VII and O VIII) while simultaneously observing lower ionization relatives in the UV (O VI, N V, and C IV). Objects with strong UV absorption lines and soft X-ray absorption are therefore good candidates for further tests of this hypothesis.

The Seyfert 1 galaxy NGC 3516 exhibits unusually strong, variable UV absorption lines (Ulrich & Boisson 1983; Voit, Shull, & Begelman 1987; Walter et al. 1990; Kolman et al. 1993; Koratkar et al. 1996), and has a variable X-ray spectrum characteristic of the warm absorber phenomenon (Halpern 1982). Observations obtained with *Ginga* (Kolman et al. 1993; Nandra & Pounds 1994) show a flat power law with energy index ~ 0.5 over the 2–18 keV range, a highly ionized iron edge with a corresponding total column density of $\sim 3 \times 10^{23}$ cm^{-2}, and a cold fluorescent Fe Kα line with EW = 377 eV.

Although the strength of the UV and X-ray absorption in both NGC 4151 and NGC 3516 suggests that the two absorbing mechanisms are related, it is not clear how. Kolman et al.'s (1993) simultaneous X-ray and UV observations of NGC 3516 were inconclusive due to a lack of variability. To measure simultaneously the X-ray and UV absorption in NGC 3516 we coordinated ASCA observations with far-ultraviolet observations using the Hopkins Ultraviolet Telescope (HUT) during the flight of the Astro-2 space shuttle mission in March 1995.

2. The ASCA Observations

Four X-ray telescopes (Serlemitsos et al. 1995) consisting of nested conical foil mirrors image X-rays onto four separate detectors in the ASCA focal plane. Two solid-state imaging spectrometers (SIS0 and SIS1), each consisting of four CCD chips, are sensitive from ~ 0.4 to 10.0 keV and have an energy resolution of $\sim 2\%$ at 6 keV (Burke et al. 1994). Two gas imaging spectrometers (GIS) cover the energy range 0.8–10.0 keV with a resolution of $\sim 8\%$ at 6 keV (Makishima et al. 1996). The observatory and its performance are described by Tanaka, Inoue, & Holt (1994).

We observed NGC 3516 twice, each time for roughly half a day with intervals lost due to source occultation by the earth and passage through the South Atlantic Anomaly (SAA). The first

observation was on 1995 March 11 from 02:24:39–14:40:48 UT. The second was from 20:03:18 UT on 1995 March 12 to 08:11:00 UT on 1995 March 13. The HUT spectra described in the next section were obtained near the mid-point of each of these intervals.

The SIS detectors were operated in FAINT 1-CCD mode, but the spectra extracted in FAINT mode showed regions of large pixel-to-pixel variations. Converting the data to BRIGHT mode eliminated these variations, and we used these spectra for the analysis presented here. Experimentation with different data screening criteria showed that bright earth avoidance angles of $> 25°$ were necessary to achieve consistent results. Default screening criteria were used for the dark earth limb angle ($> 10°$) and for the geomagnetic cutoff rigidity (> 6 GeV c^{-1}). A few high count rate

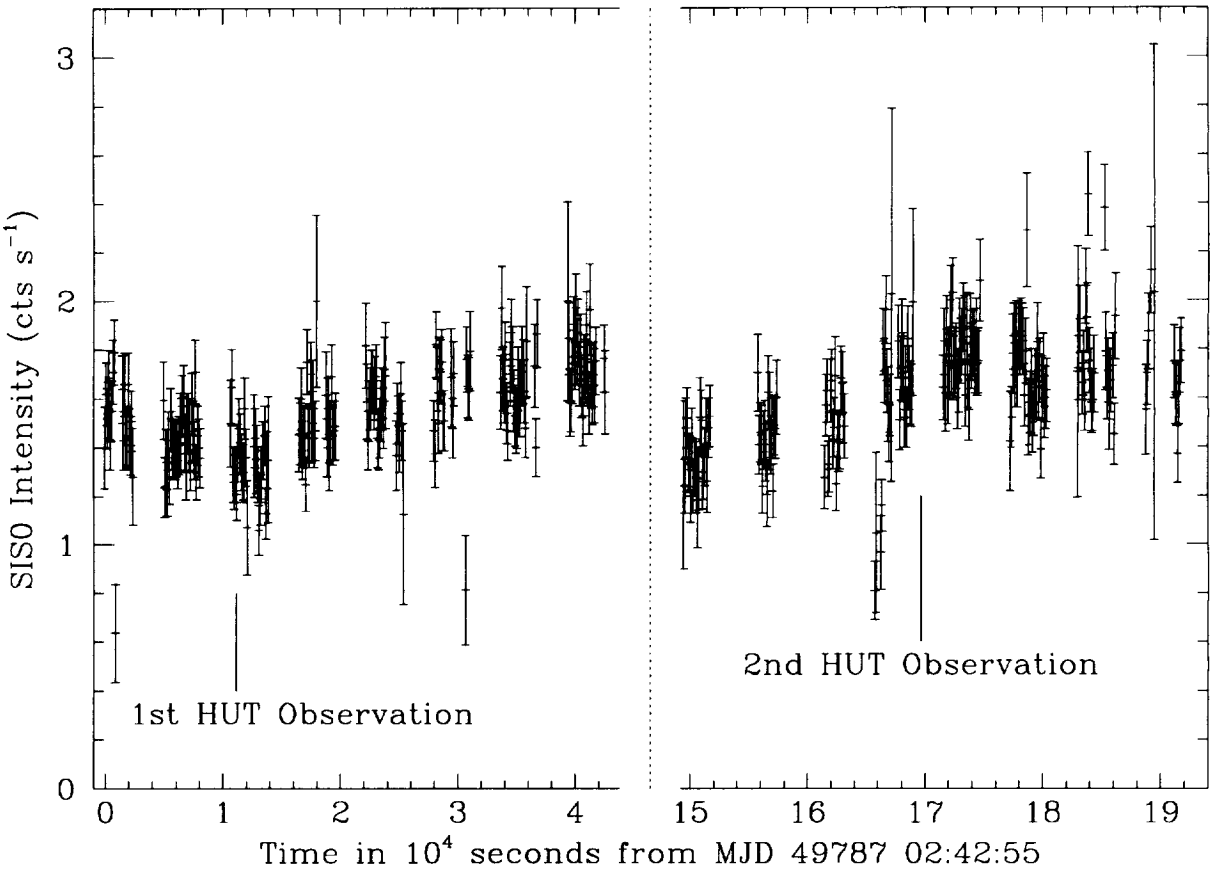

Fig. 1.— The integrated 0.4–10.0 keV count rate of NGC 3516 obtained with ASCA is shown. Time is in seconds from 02:42:55 UT on 11 March 1995. Note the break in the X-axis between the first and second observations. Data are binned into intervals of 100 s. Variations of $\sim 20\%$ are apparent on timescales of $\sim 20,000$ s. The centroids of the integration intervals for the two HUT spectra described in the next section are indicated.

intervals adjoining SAA passages were rejected by eliminating regions with count rates exceeding 2.5 cts s^{-1}. Counts for light curves and spectra were extracted from circular regions centered on NGC 3516 using the largest radius that did not extend beyond the boundary of the CCD (3′.5 for SIS0 and 2′.6 for SIS1). As shown by the SIS0 count rate in Figure 1, NGC 3516 showed intensity changes of $\sim$ 20% over the course of both observations. The combined data sets yield 54,539 events over a live integration time of 33,534 s in SIS0 and 38,935 events over 33,956 s in SIS1.

3. HUT Observations

We observed NGC 3516 on two occasions during the Astro-2 mission, once for 1518 s beginning at 5:35:34 UT on 1995 March 11, and again for 2200 s beginning at 1:32:03 on 1995 March 13. Both observations were through a 20″ aperture during orbital night when airglow is at a minimum. The basic design of HUT is described by Davidsen et al. (1992). Briefly, a 0.9-m mirror collects light for a prime-focus, Rowland-circle spectrograph. A photon-counting detector sensitive from 820–1840 Å samples the dispersed spectrum at a resolution of 2–4 Å with $\sim$0.52 Å per pixel. Improvements to HUT, its performance during the Astro-2 mission, and our basic data reduction procedures are described by Kruk et al. (1995). The raw data were reduced by subtracting dark counts, correcting for scattered geocoronal Lyα emission and subtracting airglow. We then flux-calibrated the spectrum using the time-dependent inverse sensitivity curves developed from on-orbit observations and model atmospheres of white dwarfs. Statistical errors for each pixel are calculated from the raw count spectra assuming a Poisson distribution and are propagated through the data reduction process. As there was no evidence for variability in the UV data, the two separate observations are weighted by their exposure times and combined to form the mean flux-calibrated HUT spectrum of NGC 3516 shown in Figure 2.

To model the spectrum of NGC 3516 and measure properties of the continuum, emission lines and the absorption lines, we use the IRAF task **specfit** (Kriss 1994a). We fit the continuum with a power law in f_λ. The brightest broad emission lines (O VI λ1034, Lyα, and C IV λ1549) are well described by power law profiles while single Gaussian components are adequate for the weaker broad lines. The power law profile has a functional form $F_\lambda \propto (\lambda/\lambda_o)^{\pm\alpha}$, where $\alpha = \ln 2/(1 + \mathrm{FWHM}/2c)$ (c.f. NGC 4151, Kriss et al. 1992). Additional narrow Gaussian cores are required for Lyα and He II λ1640. Single Gaussian profiles are used for all absorption lines other than the Lyman series. We allow extinction to vary freely following a Cardelli, Clayton, & Mathis (1989) curve with $R_V = 3.1$.

To model hydrogen absorption in the Galaxy and in NGC 3516, we compute grids of transmission functions including transitions up to n = 50. Using Voigt profiles of varying column density and Doppler parameter, we then convolve the transmission with the instrument resolution. Galactic neutral hydrogen is fixed at zero redshift at a column density of 3.35×10^{20} cm^{-2} (Stark et al. 1992) with a Doppler parameter of $b = 10$ km s^{-1}. A sharp, redshifted Lyman edge is readily apparent in the NGC 3516 spectrum. Neutral hydrogen intrinsic to NGC 3516 is permitted to vary freely in column density, redshift, and Doppler parameter.

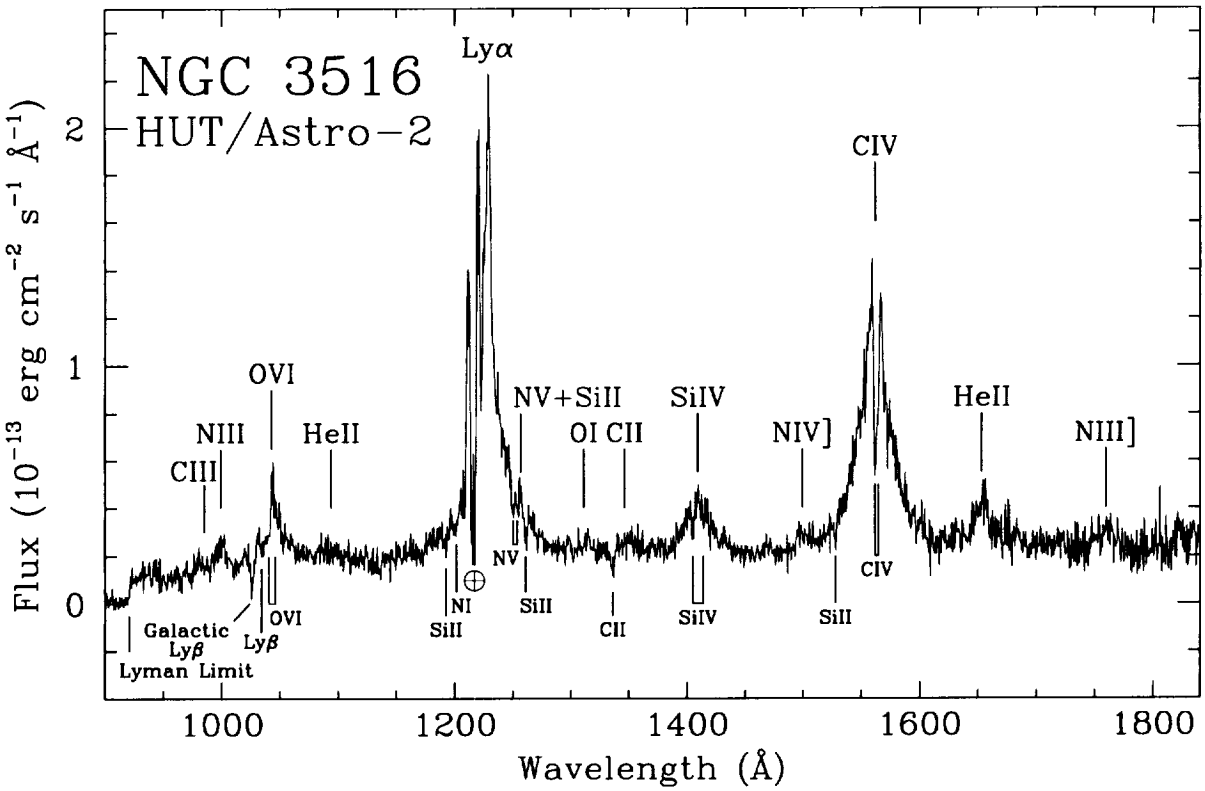

Fig. 2.— The flux-calibrated spectrum of NGC 3516 obtained with the Hopkins Ultraviolet Telescope during the Astro-2 mission is shown. Significant emission and absorption lines are marked. The indicated Lyman limit is at a redshift of 0.0075, and it is intrinsic to NGC 3516 as are the absorption lines of O VI, N V, Si IV, and C IV. The remaining absorption lines are likely galactic in origin. The earth symbol indicates the residual feature produced by subtraction of geocoronal Lyα emission.

Our best fit yields $\chi^2/\nu = 1652/1582$ for 1671 data points between 916 Å and 1800 Å (we omit a region from 1207-1222 Å surrounding geocoronal Lyα). The fitted continuum has $f_\lambda = 3.61 \times 10^{-14}\,(\lambda/1000\text{Å})^{-0.11}$ erg cm^{-2} s^{-1} Å^{-1} with $E(B-V) = 0.06 \pm 0.01$. In frequency space this corresponds to a spectral index $\alpha = 1.89$ for $f_\nu \sim \nu^{-\alpha}$. For the neutral hydrogen intrinsic to NGC 3516 we find a best fit redshift of $z = 0.0075 \pm 0.0005$, $N_{HI} = 3.5 \times 10^{17}$ cm^{-2}, and $b = 10$ km s^{-1}. This is blue-shifted by 400 ± 150 km s^{-1} relative to the 2649 km s^{-1} systemic velocity of NGC 3516 measured using the stellar absorption lines (Vrtilek & Carleton 1985). The opaque Lyman limit requires neutral hydrogen with a minimum column density $N_{HI} > 2.2 \times 10^{17}$ cm^{-2} (90% confidence). Its sharpness limits b to less than 20 km s^{-1} at 90% confidence. The general weakness of the Lyman absorption lines (only Lyα and perhaps Lyβ are detected) gives an upper limit of $N_{HI} < 6.3 \times 10^{17}$ cm^{-2} at 90% confidence.

4. Modeling the X-ray Spectrum

We used the spectral fitting program XSPEC (Shafer, Haberl, & Arnaud 1989) to model the extracted spectra. To permit the use of χ^2 statistics we grouped the data to have a minimum of 25 counts per spectral bin. This affected only bins above 6.5 keV. To avoid the worst uncertainties in the detector response, we restricted our fits to bins with energies 0.60 keV $< E <$ 9.00 keV. The SIS0 and SIS1 data were fit jointly.

Although spectral features are obvious in the raw spectrum, we first fit a simple power law with cold absorption to the data to draw a comparison with earlier X-ray observations. This model yields an energy index of 0.62, a flux at 1 keV of 0.01 photons cm^{-2} s^{-1} keV^{-1}, an equivalent neutral hydrogen column of $N_H = 1.2 \times 10^{21}$ cm^{-2} and $\chi^2/\nu = 1158/435$. The spectral shape and intensity is significantly different from that found in earlier *Ginga* observations (Kolman et al. 1993). The intensity as observed with ASCA is about twice as high, the spectral index is steeper (0.62 ± 0.03 compared to a mean of 0.47 ± 0.04 in the *Ginga* data), and the absorbing column $\sim 30\times$ lower than the value of $\sim 4.06 \pm 0.28 \times 10^{22}$ cm^{-2} found by Kolman et al. (1993). As *Ginga* is sensitive to column densities of $\sim 1 \times 10^{21}$ cm^{-2}, there is little doubt that the low energy absorption has changed significantly in character since 1989. Such striking differences in column density were seen previously in the *Einstein* observations of NGC 3516 (Halpern 1982), and they are typical of variations seen in other sources with intrinsic absorption such as NGC 4151 (Yaqoob, Warwick, & Pounds 1989; Yaqoob et al. 1993) and MR2251-178 (Halpern 1984; Otani et al. (1996)). The spectral index, however, is sensitive to the modeling of the absorption and the iron emission in the spectrum. Using the same *Ginga* data, Nandra & Pounds (1994) find a spectral index of 0.65–0.74 and absorption columns of $5.0 - 7.2 \times 10^{22}$ cm^{-2}.

The ratio of the SIS0 data to the simple power-law model shown in Figure 3 immediately reveals absorption features below 1 keV due to highly ionized oxygen and strong fluorescent emission from neutral iron around 6.3 keV. To characterize these spectral features empirically, we added a succession of Gaussian-profile emission lines and absorption edges (with opacity proportional to E^{-3}) until we obtained an acceptable fit. An acceptable description of the spectrum requires two low energy absorption edges that we attribute to O VII and O VIII, a narrow unresolved Fe Kα emission line, and a broad base to the Fe Kα line. Table 1 gives the best fit values and 90% confidence error bars for the parameters of this empirical model.

The broad and narrow Fe Kα features have a combined equivalent width (EW) of 253 ± 109 eV, comparable to the 377 ± 44 eV Fe Kα feature in the *Ginga* spectrum of Kolman et al. (1993). The energies of the oxygen edges and the narrow Fe Kα line are redshifted relative to the systemic redshift of NGC 3516 ($z = 0.008834$, Vrtilek & Carleton 1985). The O VII, O VIII, and Fe Kα features have redshifts of $z = 0.046 \pm 0.011$, $z = 0.019 \pm 0.018$, and $z = 0.016 \pm 0.0064$, respectively. Inclusion of the two oxygen edges in the fit broadens the distribution of opacity at low energies. This more accurate modeling of the shape of the low energy absorption leads to a spectral index of 0.78 that is steeper than that in the simple power-law fit and is more comparable to the mean

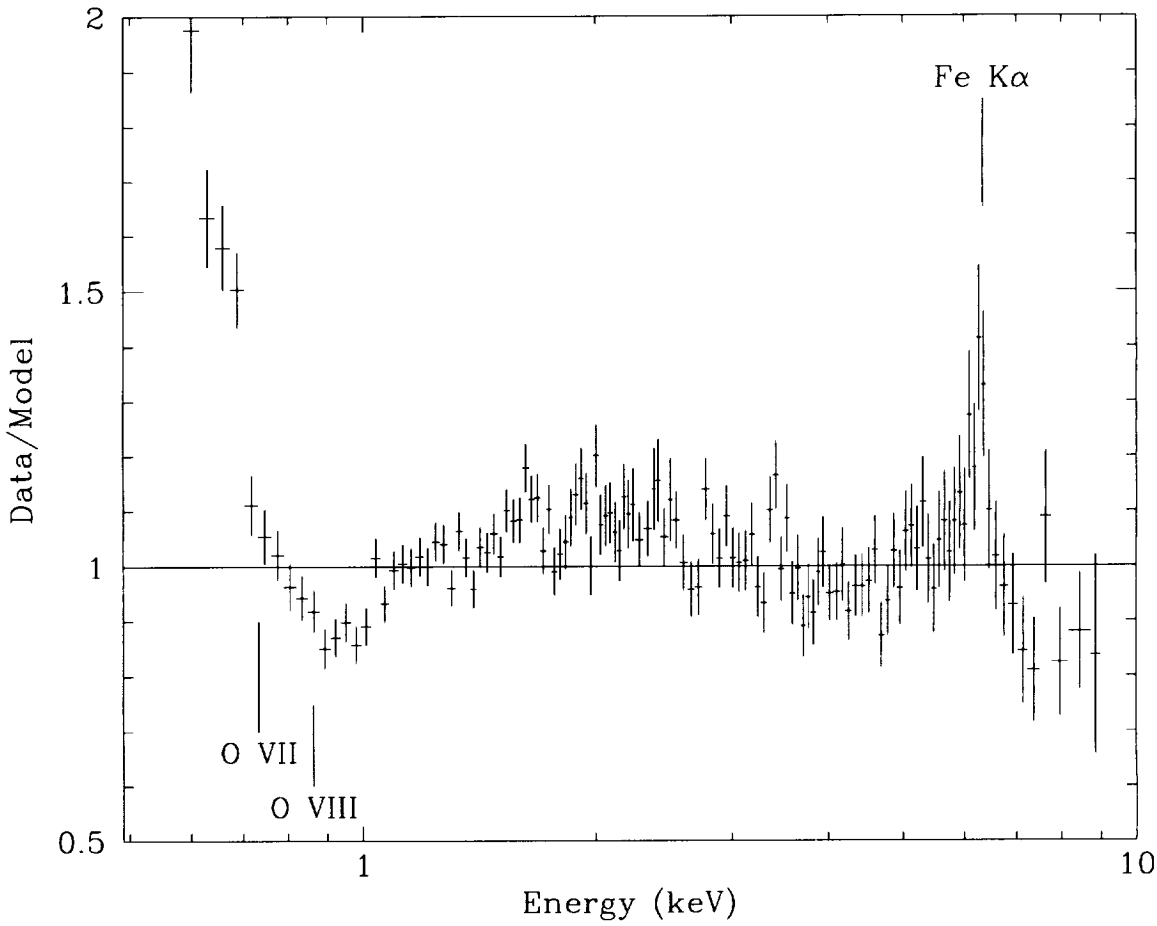

Fig. 3.— To illustrate the features present in the X-ray spectrum of NGC 3516, the data were divided by a simple model consisting of a power law with low energy absorption by neutral gas. The ratio of the data to the model shows a prominent absorption dip around the photoionization edges of O VII and O VIII as well as complex structure around the iron Kα line.

power law index of 0.73 found for *Ginga* observations of Seyferts (Nandra & Pounds 1994). The residual absorption by cold gas of $N_{HI} = 6.8 \times 10^{20}$ cm^{-2}, however, is still higher than the expected Galactic column of $N_H = 3.35 \times 10^{20}$ cm^{-2} (Stark et al. 1992). At first glance it might seem natural to attribute this excess above the Galactic column to cold gas intrinsic to NGC 3516. However, the far-UV spectrum obtained with HUT limits the intrinsic neutral hydrogen column in NGC 3516 to $< 8 \times 10^{17}$ cm^{-2} based on the strengths of the observed Lyman lines and Lyman limit. The most likely explanation for the observed excess cold column is the uncertainty in the ASCA calibration below 1 keV. These uncertainties can lead to excess column densities of up to 3×10^{20} cm^{-2}.

Iron edges are also important diagnostics of the ionization state of the absorbing medium. No iron edge feature is apparent in the residuals from our fit, and this is not surprising given the

order-of-magnitude lower columns we are seeing relative to earlier X-ray observations of NGC 3516. Adding an additional sharp edge with its energy constrained to be greater than 7.1 keV gives no improvement in χ^2. The optical depth at the edge must be less than 0.3 at the 90% confidence level.

The moderately strong edges of highly ionized oxygen in our spectrum naturally suggest an origin in photoionized gas. The dominant strength of the O VII edge indicates gas of much lower ionization and temperature than that modeled by Krolik & Kriss (1995), and the absence of an Fe K edge indicates a much smaller column. Accordingly we have computed new models that span the potential range of ionization parameters and column densities with some slight modifications to the procedure described by Krolik & Kriss (1995). First, we used an ionizing spectrum appropriate for NGC 3516 at this epoch. The best-fit UV power law of $f_\nu \sim \nu^{-1.89}$ from the HUT spectrum

Table 1. Empirical Model Parameter Values

Parameter	Value[a]
N_{HI} (10^{20} cm^{-2})[b]	6.8 ± 1.0
Edge Energy E_1 (keV)	0.707 ± 0.008
Optical Depth τ_1	0.65 ± 0.07
Edge Energy E_2 (keV)	0.855 ± 0.015
Optical Depth τ_2	0.31 ± 0.05
Energy index α	0.776 ± 0.029
Normalization (phot cm^{-2} s^{-1} keV^{-1})	0.0126 ± 0.00037
Narrow Fe Energy (keV)[c]	6.293 ± 0.040
Narrow Fe EW (eV)	73 ± 27
Broad Fe Energy (keV)	5.88 ± 0.37
Broad Fe EW (eV)	180 ± 106
Broad Fe FWHM (keV)	1.58 ± 0.84
χ^2/ν	494.7/426[d]

[a] The quoted errors are 90% confidence for a single interesting parameter.

[b] Equivalent neutral hydrogen column for absorption by cold (neutral) gas.

[c] The intrinsic width of this unresolved line was held fixed at 0 eV. The 90% confidence upper limit on the line FWHM is 39 eV.

[d] The probability of exceeding χ^2 in this fit is 0.012.

was extrapolated to higher frequencies, and the best-fit X-ray power law for the ASCA spectrum, $f_\nu \sim \nu^{-0.78}$, was extrapolated to lower frequencies; the two meet at 51 eV. Second, the lower temperatures and ionization state place the gas in a regime where thermal equilibrium is more likely because the cooling time is rather shorter. We therefore compute our models in thermal equilibrium. Finally, for ease of comparison to warm absorber models fit to the X-ray spectra of other AGN, we assume constant density clouds and use the ionization parameter $U = n_{ion}/n_H$, where n_{ion} is the number density of ionizing photons between 13.6 eV and 13.6 keV illuminating the cloud and n_H is the density of hydrogen atoms.[1] The transmission of each model is computed exactly as described by Krolik & Kriss (1995), taking into account resonant line scattering and electron scattering as well as continuum opacity. The resulting models are a two parameter family in total column density N and ionization parameter. These are read into XSPEC as a FITS table for fitting to the X-ray spectrum.

As in Krolik & Kriss (1995) we assume low density gas ($n_H = 10^3$ cm^{-3}), but there are no density-dependent effects in our calculations or results, provided one considers densities lower than $\sim 10^{11}$ cm^{-3}. Although the UV continuum in our photoionizing spectrum is steep, we note that there is no lack of high energy photons. The spectrum flattens just below the He II edge to $f_\nu \sim \nu^{-0.78}$, and the overall $\alpha_{ox} = 1.20$, a value typical of Seyfert 1 galaxies (Kriss & Canizares 1985). In fact, tests show that our results are rather insensitive to the exact shape of the ionizing spectrum apart from changes in the deduced ionization parameter. (This is a general property of photoionization models with broad distributions of ionizing flux noticed in even the earliest calculations [Tarter, Tucker, & Salpeter 1969].) For comparison we computed alternative models assuming either an extremely hard spectrum with $f_\nu \sim \nu^{-0.78}$ from 2500 Å through the UV and X-ray up to 100 keV, or the spectral shape of NGC 5548 as used by Mathur et al. (1995), which contains a soft X-ray excess. Neither of these match the observed broad-band spectral shape, yet they both provide equally good descriptions of the opacity of the warm absorber.

The Fe Kα lines in our empirical fit to the ASCA spectrum are indicative of fluorescent emission. As a better model for the X-ray continuum shape we therefore use that predicted by Lightman & White (1988) for a disk illuminated by a power law. Our data do not constrain the inclination or the solid angle subtended by the disk, so we fix these parameters at 30° and 2π, respectively. The source is assumed to radiate isotropically, and we impose a high energy cutoff of 300 keV on the intrinsic power law.

Using the optical depths given by our best empirical fit in Table 1 and the threshold photoionization cross sections of Verner & Yakovlev (1995), we infer column densities for O VII and O VIII of 3.5×10^{18} cm^{-2} and 2.6×10^{18} cm^{-2}, respectively. Assuming these represent all the oxygen atoms, the equivalent total hydrogen column for a solar abundance of oxygen is 9.3×10^{21} cm^{-2}. Replacing the two oxygen edges in our empirical model with the grid of warm absorber models,

---

[1]For comparison to the constant-pressure models of Krolik & Kriss (1995), the ionization parameter $\Xi = P_{rad}/P_{gas} = 5.3\ U$ for gas at 10^5 K.

for the best fit we obtain a column density and ionization parameter that qualitatively matches our expectations, as shown in the center column of Table 2. This fit is only slightly worse than our empirical model. Warm absorber models computed with our alternative ionizing spectra give identical best fit values for the total column density ($\log N = 22.02$). For the hard $\nu^{-0.78}$ spectrum the best-fit ionization parameter is $U = 0.25$ with $\chi^2/\nu = 501.5/427$, and for the spectrum like NGC 5548, $U = 1.71$ with $\chi^2/\nu = 500.7/427$.

Table 2. Warm Absorber Model Parameters

Parameter	Single Absorber[a]	Two Absorbers[a]
N_{HI} (10^{20} cm^{-2})[b]	7.1 ± 1.7	7.7 ± 1.6
Ionization Parameter U_1	0.48 ± 0.06	1.66 ± 0.31
log Total Column Density N_1	22.02 ± 0.06	22.15 ± 0.12
Redshift z_1	0.037 ± 0.011	0.007 ± 0.014
Ionization Parameter U_2	...	0.32 ± 0.11
log Total Column Density N_2	...	21.84 ± 0.04
Redshift z_2	...	0.050 ± 0.013
Intrinsic Energy index α[c]	0.97 ± 0.08	1.05 ± 0.07
Normalization (phot cm^{-2} s^{-1} keV^{-1})	0.0167 ± 0.0014	0.0191 ± 0.0020
Narrow Fe Energy (keV)[d]	6.289 ± 0.039	6.294 ± 0.038
Narrow Fe EW (eV)	76 ± 29	79 ± 30
Broad Fe Energy (keV)	5.91 ± 0.33	6.00 ± 0.34
Broad Fe EW (eV)	387 ± 170	427 ± 171
Broad Fe FWHM (keV)	2.33 ± 0.63	2.47 ± 0.89
χ^2/ν	500.7/427[e]	486.5/424[f]

[a] The quoted errors are 90% confidence for a single interesting parameter.

[b] Equivalent neutral hydrogen column for absorption by cold (neutral) gas.

[c] This is the intrinsic energy index for a power-law spectrum illuminating a cold disk of gas. The inclination of the disk is fixed at 30° and its covering fraction is fixed at 2π.

[d] The intrinsic width of this unresolved line was held fixed at 0 eV.

[e] The probability of exceeding χ^2 in this fit is 0.0079.

[f] The probability of exceeding χ^2 in this fit is 0.019.

As discussed below, the strengths of the UV absorption lines observed in NGC 3516 require a zone of lower ionization and lower column density than this warm-absorber model. Other observations also indicate that the warm absorbing medium may be complex. Otani et al. (1996) find that the O VIII opacity in MCG–6-30-15 is variable, while the O VII opacity is not, suggesting that the absorption arises in at least two different zones. Prompted by these suggestions of spectral complexity, we experimented with adding a second warm absorber to the fit. This significantly improves χ^2. Although the level of improvement is not sufficient to be apparent in any particular feature in the spectrum, an F test for 3 additional parameters producing $\Delta\chi^2 = 14.2$ shows that this second model component is significant at the 99% confidence level. The parameters of this best fit are summarized in the last column of Table 2. The SIS0 and SIS1 spectra and this best fit model are illustrated in the top panel of Figure 4.

As in Krolik & Kriss (1995) all the warm absorber models above assumed resonant line scattering profiles with Doppler parameters given by the sound speed in the photoionized gas. Since the line opacity is sensitive to the assumed profile width, it influences the transmission computed for each model. At low velocities the opacity is dominated by continuum absorption; at high velocities resonant line scattering makes a significant contribution. To illustrate, Figure 5 shows the computed transmission for $b = 200$ km s^{-1} divided by that for $b = 10$ km s^{-1}. Physical parameters as determined by the best-fit single absorber model in Table 2 were used for the ionization parameter and column density. The upper panel shows the ratio of the models themselves. The lower panel shows the ratio after the models have been folded through the ASCA response function. The error bars on each bin are taken from the corresponding data points.

The stronger predicted line absorption at $b = 200$ km s^{-1} is clear. Below 1 keV O VIII and Fe-L transitions dominate the increased opacity. The only significant features above 1 keV are the resonance transitions of Mg XI and Si XIII. At $b = 10$ km s^{-1} the absorption lines have an integrated equivalent width of 5 eV and make a negligible contribution to the total opacity, whereas at $b = 200$ km s^{-1} their equivalent width is 42 eV and 6% of the opacity between 0.6 and 2.0 keV is due to line absorption.

Within the context of our photoionization models the dependence of line opacity on line width permits us to constrain the Doppler parameter, even though discrete absorption lines are not unambiguously present in the observed spectrum. In essence we find that the *absence* of significant resonant absorption line features permits us to set upper limits on the Doppler parameter. We computed grids of models with Doppler parameters varying from 10 km s^{-1} to 200 km s^{-1}. The best fits for both the single and the double warm absorber have Doppler parameters of 50 km s^{-1}, approximately the sound speed for these models. (For the double warm absorber model we used the same Doppler parameter for each component.) At 90% confidence for a single interesting parameter ($\Delta\chi^2 = 2.706$) we constrain the Doppler parameter to values less than 160 km s^{-1} for the single warm absorber model, and to less than 120 km s^{-1} for the model with two warm absorbers.

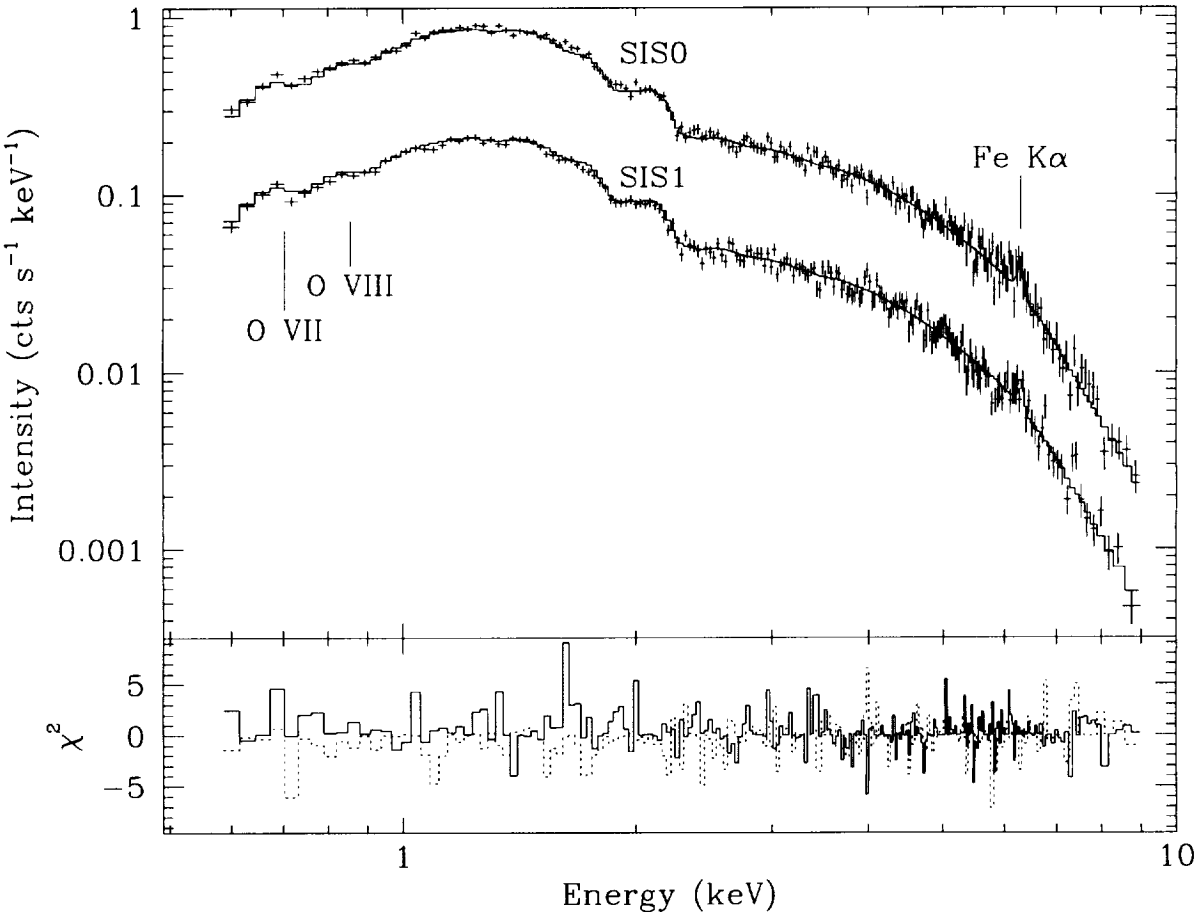

Fig. 4.— *Upper Panel:* The solid lines are the best-fit empirical model folded through the ASCA SIS0 and SIS1 detector responses. The data points are crosses with 1σ error bars. The SIS1 data are offset down by 0.5 in the log for clarity. The model includes a power law with photon index 1.78, absorption by neutral gas with an equivalent neutral hydrogen column of $N_H = 6.8 \times 10^{20}$ cm^{-2}, a photoionization edge due to O VII at 0.71 keV with an optical depth at the edge of 0.65, a photoionization edge due to O VIII at 0.86 keV with optical depth 0.31, an unresolved iron Kα line at 6.29 keV with an equivalent width of 73 eV, and a broad (FWHM = 1.58 keV) iron Kα line at 5.88 keV with an equivalent width of 180 eV. *Lower Panel:* The contributions to χ^2 of each spectral bin are shown. The solid line is for SIS0 and the dotted line for SIS1.

5. The Complex Absorbing Medium in NGC 3516

Intrinsic UV absorption lines are prominent in the HUT spectrum of NGC 3516, but they are near the weakest levels seen in NGC 3516, comparable to their appearance in the 1993 IUE monitoring campaign (Koratkar et al. 1996). The frequently observed blue-shifted absorption trough (Voit, Shull, & Begelman 1987; Walter et al. 1990; Kolman et al. 1993) is not present,

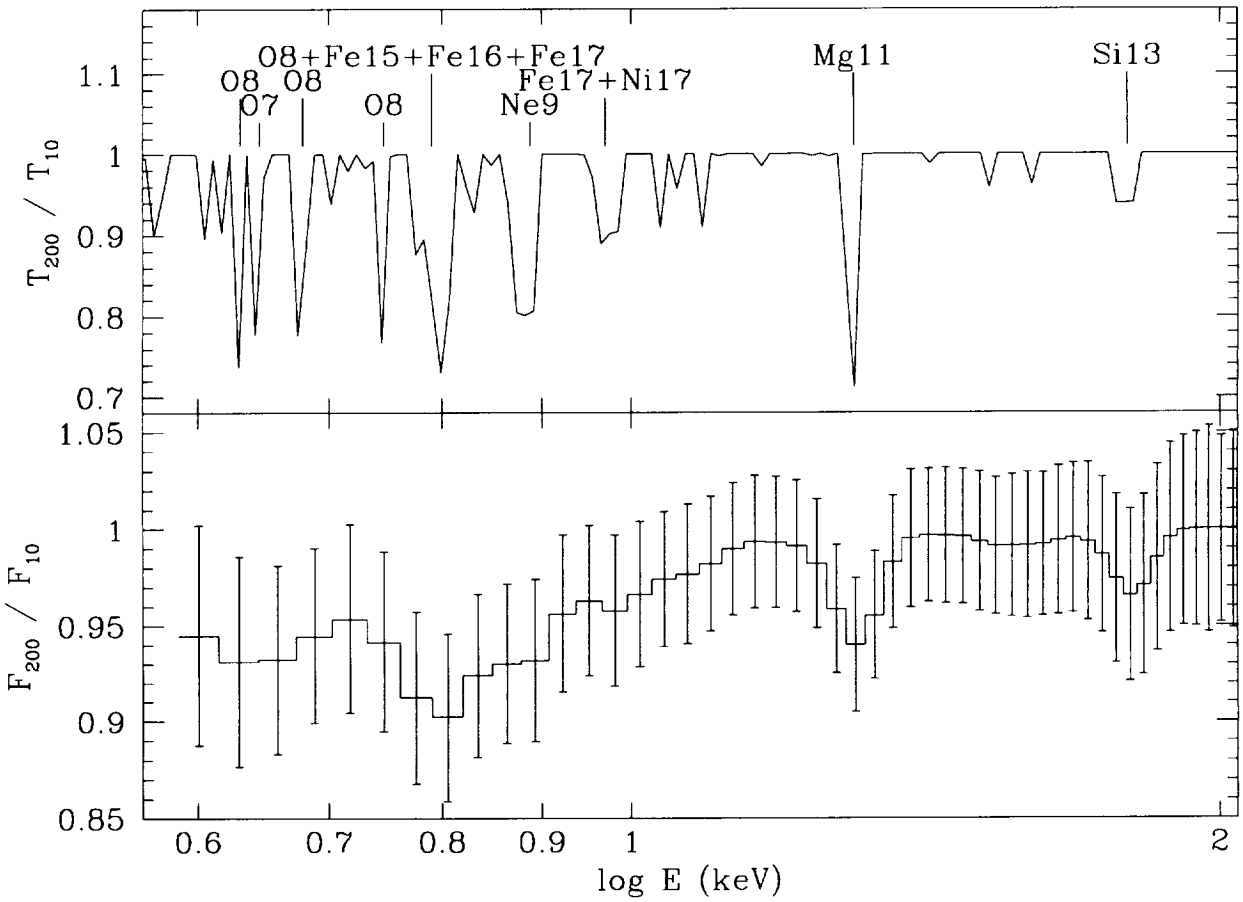

Fig. 5.— *Top Panel:* The ratio of the transmission for a warm absorber model with absorption lines broadened by a Doppler parameter of b = 200 km s^{-1} to the same model broadened with b = 10 km s^{-1}. Physical parameters as determined by the best-fit single absorber model in Table 2 were used for the ionization parameter and column density. Ion species contributing to the most significant lines are marked. *Lower Panel:* Here the models are folded through the ASCA response function before computing the ratio. The error bars on each bin are taken from the corresponding data at that point.

and the C IV feature in our spectrum probably corresponds to the narrow component in the models of Walter et al. (1990). Although the C IV absorption line in the HUT spectrum is narrow, it is resolved. After correcting for instrumental broadening by subtracting a 2.0 Å Gaussian in quadrature (Kruk et al. 1995), we find an intrinsic width for the line of 350 km s^{-1}. This corresponds to b = 210 km s^{-1}, which is consistent with the observed equivalent widths (EWs) and optically thin doublet ratio of the deblended C IV lines. The other high ionization resonance lines also have optically thin doublet ratios consistent with $b \sim 200$ km s^{-1}. In contrast, the neutral hydrogen absorption at the Lyman limit requires $b < 20$ km s^{-1}. This, and the significantly

different velocity of the neutral hydrogen absorption, are indications that the absorbing medium contains multiple zones.

Our simultaneous X-ray observations of NGC 3516 discussed in the previous section also hint that the absorbing medium may be complex. This is in contrast to the single-zone photoionization models that match the X-ray and UV absorption seen in 3C 351 (Mathur et al. 1994) and in NGC 5548 (Mathur, Wilkes, & Elvis 1995). We now test in more detail whether this is true for NGC 3516. The single warm absorber fit to the ASCA spectrum of NGC 3516 has $U = 0.48$ and $\log N = 22.02$. Given the column densities predicted by this model for the UV ions, we can place the observed EWs on curves of growth (Figure 6). If the model self-consistently accounts for both the X-ray and UV absorbers, all the plotted EWs should lie on a single curve of growth. As shown in the top panel of Figure 6, they do not. The predicted column densities of neutral hydrogen and Si IV are orders of magnitude below what we observe in the HUT spectrum, and a single Doppler parameter does not give a good match to the remaining UV lines. Choosing $b = 70$ km s^{-1} fits the N V and O VI doublets within the errors, but this underpredicts the strength of the C IV doublet by factors of several. This situation is similar to the difficulties noted by Kriss et al. (1995) in trying to account for the low-ionization UV absorption lines in NGC 4151 with a single warm absorber model.

We also considered alternative ionizing continua to test the sensitivity of our results to the assumed incident spectrum. We used both an extremely hard spectrum with $f_\nu \sim \nu^{-0.78}$ from 2500 Å through the UV and X-ray up to 100 keV, and also the spectral shape of NGC 5548 as used by Mathur et al. (1995), which contains a soft X-ray excess. The models are computed for constant density ($n_H = 10^3$ cm^{-3}) clouds in thermal equilibrium. (For densities $< 10^{11}$ cm^{-3} there are no density-dependent effects in our calculations or results.) The models are described by their ionization parameter U and their total column density N. These alternative models give similar results, with the predicted columns of the UV ions in each model within tens of percent of each other. This insensitivity to the precise shape of the ionizing spectrum is not surprising. For broad ionizing continua such as power laws or broken power laws, even the earliest photoionization calculations (e.g., Tarter, Tucker, & Salpeter 1969) showed that models were much more sensitive to ionization parameter than to spectral shape. In Table 3 we compare the columns inferred from the UV absorption lines assuming they are optically thin, as indicated by their doublet ratios, to the column densities predicted by the various models. The similarity of the models to each other is apparent, as is the large disagreement with the observations, particularly for Si IV.

The two-component warm absorber fit favored by the ASCA data also fails as an adequate description of the UV absorption. The lower ionization zone with $U = 0.32$ and $\log N = 21.84$ still falls short in matching the Si IV and H I by orders of magnitude, and once again a single Doppler parameter fails to match the observations of the remaining UV lines. The only UV-absorbing species with a significant column at any Doppler parameter in the higher ionization zone ($U = 1.66$, $\log N = 22.15$) is O VI.

Producing the observed EWs of the UV lines requires regions of lower ionization and lower

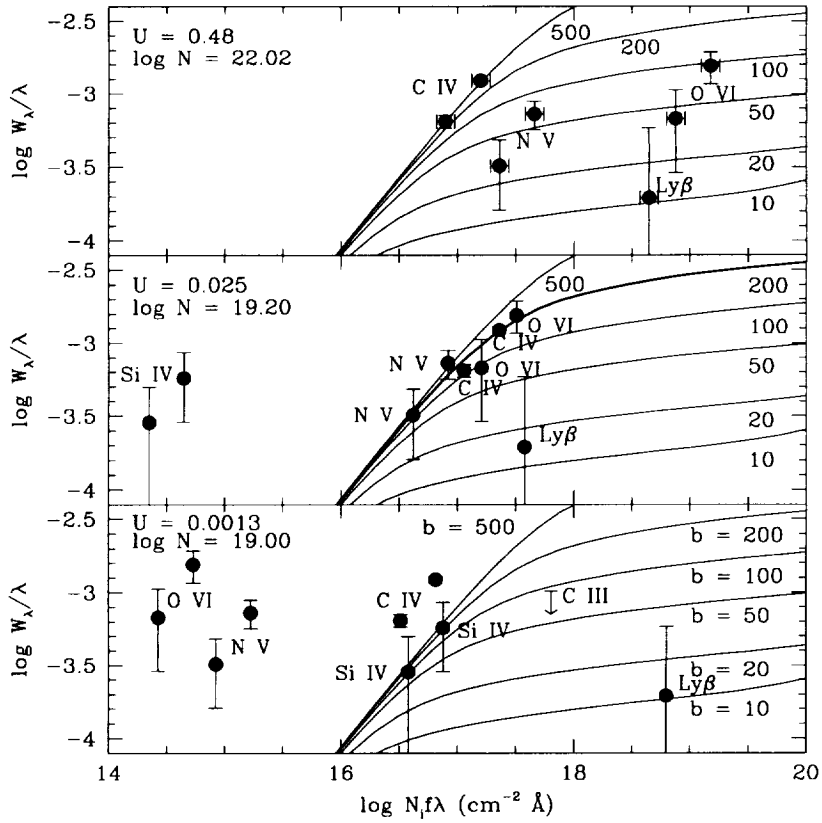

Fig. 6.— *Top Panel:* The observed EWs of the UV absorption lines in NGC 3516 are plotted on curves of growth using column densities predicted by the single warm absorber fit to the ASCA X-ray spectrum. This model has $U = 0.48$ and a total column density of $10^{22.02}$ cm^{-2}. Points are plotted at a horizontal position determined by the column density for the given ion in the model with a vertical coordinate determined by the observed EW for the corresponding absorption line. The vertical error bars are from Table 2, and the horizontal error bars are the range in column density allowed by the uncertainty in the fit to the ASCA spectrum. The predicted column of Si IV in this model is too low to appear on the plot. The thin solid lines show predicted EWs as a function of column density for Voigt profiles with Doppler parameters of b = 10, 20, 50, 100, 200, and 500 km s^{-1}. A model that fits the data would have all points lying on one of these curves. This model cannot simultaneously match both the UV and the X-ray absorption. *Center Panel:* The observed EWs are plotted for column densities predicted by a model with $U = 0.025$ and a total column density of $10^{19.2}$ cm^{-2}. The heavy solid curve at $b = 200$ km s^{-1} gives a good match to the observed EWs of the C IV, N V, and O VI doublets, but the predicted EW of Si IV is far below the observed value. *Bottom Panel:* The observed EWs are plotted for column densities predicted by a model with $U = 0.0013$ and $N = 10^{19.0}$ cm^{-2}. $b = 20$ km s^{-1} can match the observed EWs of Si IV and Lyβ and satisfy the upper limit on the EW of C III λ977.

column density than those producing the X-ray absorption. For $U = 0.025$, $\log N = 19.2$ cm^{-2},

and b = 200 km s^{-1} we find a good match to the observed EWs of the C IV, N V, and O VI doublets as shown in the center panel of Figure 6. The predicted EW of the Lyβ line is $\sim 2\sigma$ higher than observed, but enhancing the overall metal abundance by a factor of a few can correct this. However, the predicted EW of Si IV in this model is orders of magnitude below the observed value. Similar problems are encountered in matching the inferred column densities of Si IV absorption in models of broad-absorption line (BAL) QSOs (Weymann, Turnshek, & Christiansen 1985). *Ad hoc* adjustments to the ionizing continuum can alleviate the disagreement to some extent (Weymann, Turnshek, & Christiansen 1985), but even the most extreme changes do not bring the predictions within the bounds of the observations, again showing the relative insensitivity of photoionization models to the shape of the ionizing spectrum. Producing enough Si IV absorption requires a zone of even lower ionization. Choosing U = 0.0013 and $\log N$ = 19.0 matches the Si IV EWs without contributing much to the columns of the higher ionization lines. This model is illustrated in the lower panel of Figure 6. Limits on the EWs of lower ionization species such as Lyβ and C III λ977, however, require b < 50 km s^{-1}. This lower ionization zone with low Doppler parameter is potentially the origin of the optically thick Lyman limit system, but the predicted column of neutral hydrogen in this model is only $N_{HI} = 7.7 \times 10^{16}$ cm^{-2}, a factor of 4 below the observed value.

Table 3. Observed and Predicted Absorption Columns in NGC 3516

Ion	N_{obs}[a] (cm^{-2})	N_{Model1}[b] (cm^{-2})	N_{Model2}[c] (cm^{-2})	N_{Model3}[d] (cm^{-2})
H I	3.5×10^{17}	5.0×10^{16}	1.7×10^{17}	1.8×10^{16}
C IV	4.7×10^{14}	4.7×10^{14}	6.0×10^{14}	5.4×10^{14}
N V	4.1×10^{14}	2.1×10^{15}	2.5×10^{15}	3.2×10^{15}
O VI	1.3×10^{15}	9.8×10^{16}	1.1×10^{17}	1.4×10^{17}
Si IV	1.1×10^{14}	$< 1 \times 10^{10}$	$< 1 \times 10^{10}$	$< 1 \times 10^{10}$

[a]Column density assuming the observed absorption lines are optically thin. The H I column is from the Lyman-limit fit.

[b]Predicted column density for the single-zone warm absorber model with the NGC 3516 ionizing spectrum, U = 0.48 and log N = 22.02.

[c]Predicted column density for the warm absorber model with the $\nu^{-0.78}$ ionizing spectrum, U = 0.16 and log N = 22.02.

[d]Predicted column density for the warm absorber model with the NGC 5548 ionizing spectrum, U = 1.47 and log N = 22.02.

The multiple zones considered above span a range of 10^3 in both column density and ionization parameter, and they form a nearly orthogonal set that makes it possible to consistently model the UV and X-ray absorption with separate regions of gas in very different physical states. For Doppler parameters at the sound speed of the two high ionization zones producing the X-ray absorption (30 km s^{-1} in the lower ionization zone, 70 km s^{-1} in the higher), the predicted contribution of the X-ray absorbing gas to the EWs of the C IV, N V, and O VI lines is only 20–30% of their observed values. The UV zones producing the C IV, N V, O VI and Si IV lines have total columns with negligible impact on the X-ray opacity. Since the X-ray absorbing gas is predicted to have a significantly lower Doppler parameter than the gas producing the bulk of the UV absorption lines, high resolution spectra in the UV should be able to identify kinematic components associated with the different zones.

Several previous authors have suggested that the UV absorption lines and the X-ray absorption seen in some AGN may have a common origin in BELR clouds (Ferland & Mushotzky 1982; Reichert, Mushotzky, & Holt 1986). However, Mathur et al. (1994) show that the physical conditions of the UV and X-ray absorber in 3C 351 are different from those of the BELR clouds, with the X-ray warm absorber requiring a much higher ionization parameter than the clouds producing the broad emission lines. For NGC 3516, Voit, Shull, & Begelman (1987) argued that the observed absorption profile (the C IV absorption in the 1980's was much broader and stronger than observed here) required 10–30 BELR clouds along the line of sight and that photoionized C IV could not be present in the outer clouds due to shielding by the inner ones. The lack of observed Mg II absorption was another difficulty for models involving BELR clouds. They concluded that the absorption must arise in optically thin, outflowing material with a density exceeding 10^5 cm^{-3}, given the observed variability, and that it could not be associated with typical BELR clouds.

Our conclusions are similar, even though the absorption is now much weaker. The ionization parameter we derive for the broad emission-line clouds ($U \sim 0.035$) is an order of magnitude lower than that required by the X-ray absorbing gas, making it highly unlikely that the X-ray absorption occurs in BELR clouds. $U \sim 0.035$, however, is similar to the ionization parameter we find for the zone producing the C IV, N V, and O VI absorption lines ($U \sim 0.025$). Although these absorption lines and the broad emission lines share comparable ionization parameters, the total columns of the BELR clouds are $\sim 10^3\times$ higher, as the broad emission line clouds are optically thick in these transitions, but the absorbing clouds are optically thin. This column density constraint is a poor one, however, because the BELR is highly stratified, and there may well be a population of clouds that both make the absorption lines and contribute to the broad-line emission. The velocity distribution of such clouds would have to be rather peculiar, however, to project a velocity width of only 200 km s^{-1} along the line of sight from an ensemble with an emission line width of $\sim$ 4000 km s^{-1}. We conclude that we still cannot unambiguously establish the location of the absorbing gas, but it must be physically distinct from the broad emission line clouds.

Although we have described the UV and X-ray absorbing zones as discrete entities, it is quite likely that there is a broad, possibly continuous, distribution of parameters such as one might find

in an outflowing wind, either from the accretion disk or from the surface of the obscuring torus. NGC 3516 is one of the rare Seyfert 1 galaxies that shows an extended, biconical NLR (see Golev et al. 1995 for the best images). Among Seyfert 1's, only NGC 4151 has such an extensive NLR with a biconical morphology (Pogge 1989; Evans et al. 1994; Schmitt & Kinney 1996). The biconical morphology in NGC 3516 implies that our line of sight passes close to the surface of the obscuring torus as suggested for NGC 4151 by Evans et al. (1993). The opaque Lyman limit is another characteristic that NGC 3516 shares with NGC 4151. These features are unusual in combination for a Seyfert 1, and their presence in yet another galaxy strengthens the case for collimation of the ionizing radiation by the absorbing gas.

The complexity of the UV and X-ray absorption that both NGC 3516 and NGC 4151 exhibit suggest that the inclination of the source relative to the observer may lead to the differences between these two objects and the apparently simpler cases considered by Mathur et al. (1994,1995). The simpler warm absorbers with only high-ionization UV absorption lines may be viewed at higher inclination, further away from the denser medium near the torus. Such geometrical differences may ultimately help us to understand the location and origin of the warm absorbing gas in AGN.

6. Summary

The broad Fe Kα emission line in our spectrum of NGC 3516 resembles features seen in MCG–6-30-15 (Tanaka et al. 1995; Fabian et al. 1995), in NGC 5548 and IC 4329A (Mushotzky et al. 1995) and in NGC 4151 (Yaqoob et al. 1995). At the signal-to-noise ratio of our spectrum we are unable to place significant constraints on relativistic disk models. In fact, the width and luminosity of the line depends strongly on our model for the underlying continuum. In the empirical model, summarized in Table 1, the line width is smaller largely because the underlying continuum is flatter and has less curvature than in the warm absorber models. In the warm absorber models the widths and equivalent widths are large, but given the uncertainties, they are compatible with the maximum equivalent widths of $\sim$ 200 eV expected in models of X-ray reflection from cold disks (e.g., George & Fabian 1991).

A simple, single-zone photoionized absorber is an imperfect description of the soft X-ray opacity in NGC 3516. At least two zones are required to give as good a fit to the ASCA data as our empirical model containing discrete absorption edges due to O VII and O VIII. These two zones may be a simplification of a broad distribution of ionization parameters in the absorbing gas, or they may be indicative of two entirely different regions as suggested by Otani et al. (1996) in their study of the variability of O VII and O VIII opacity in MCG–6-30-15. The complexity of the absorbing gas in NGC 3516 increases even more when one considers the UV absorption lines observed simultaneously with HUT. Neither a single photoionized absorber nor multiple warm absorber models are adequate to explain the UV absorption lines. This confirms the conclusion of Kolman et al. (1993) that there is probably not a direct connection between the warm X-ray and the UV absorbers in NGC 3516.

Having separate regions for the X-ray and UV absorption contrasts with the conclusions of Mathur et al. (1994,1995) in their studies of the warm absorbers in 3C 351 and in NGC 5548. For those objects they described a single absorbing zone that could account for both the X-ray warm absorber and the associated UV absorption lines. Not all X-ray and UV absorbers may be so simple. A clue to the additional complexity of the absorption in NGC 3516 is the presence of large columns of lower ionization species such as Si IV and an optically thick Lyman limit. Low ionization species also present problems for single zone models in attempting to model UV and X-ray absorption in NGC 4151 (Kriss et al. 1995). Since Si IV absorption is strong in broad absorption line quasars, by analogy this may indicate that single zone models will also not suffice to explain both the UV and X-ray absorption in these objects, contrary to the suggestion of Mathur, Elvis, & Singh (1995).

Although the absorbing medium in NGC 3516 appears to be highly stratified, the presently observed weak X-ray absorption coincident with an episode of weak UV absorption suggests that some underlying mechanism ties them together. At the epoch of our observation, NGC 3516 was brighter than usual by about a factor of two, but the low energy X-ray absorption decreased by more than can be accounted for simply by photoionization due to the increased luminosity. As suggested by Walter et al. (1990), these large changes in absorption column may be caused by different clouds moving across the line of sight. Rather than a single cloud, however, we require a whole population of clouds of differing column densities and ionization parameters moving into place. If the absorption arises in a wind driven from the accretion disk or the obscuring torus, large changes in opacity that are correlated in the UV and the X-ray may be linked by fluctuations in the mass supply to the outflow. X-ray and UV absorption in AGN may ultimately have a common origin, but the absorption probably occurs in distinctly different regions with a variety of physical conditions.

REFERENCES

Burke, B. E., et al., 1994, IEEE Trans. Nuc. Sci., 41, 375

Evans, I. N., Ford, H. C., Kriss, G. A., & Tsvetanov, Z. 1994, in The First Stromlo Symposium: The Physics of Active Galaxies, ASP Conf. Ser. 54, ed. G. V. Bicknell, M. A. Dopita, & P. J. Quinn, (San Francisco: ASP), p. 3

Evans, I., Tsvetanov, Z., Kriss, G. A., Ford, H. C., Caganoff, S., & Koratkar, A. P. 1993, ApJ, 417, 82

Fabian, A. C., et al. 1994, PASJ, 46, L59

Fabian, A. C., et al. 1995, MNRAS, in press

Ferland, G. J., & Mushotzky, R. F. 1982, ApJ, 262, 564

George, I., & Fabian, A. C. 1991, MNRAS, 249, 352

Halpern, J. P., 1982, Ph.D. thesis, Harvard University

Halpern, J. P., 1984, ApJ, 281, 90

Holt, S. S., et al. 1980, ApJ, 241, L13

Lightman, A. P., & White, T. R. 1988, ApJ, 335, 57

Kolman, M., Halpern, J. P., Martin, C., Awaki, H., & Koyama, K. 1993, ApJ, 403, 592

Koratkar, A., et al. 1996, in preparation

Kriss, G. A. 1994, in Astronomical Data Analysis Software and Systems III, ASP Conf. Ser. 61, ed. D. R. Crabtree, R. J. Hanisch, & J. Barnes, (San Francisco: ASP), 437

Kriss, G. A., & Canizares, C. R. 1985, ApJ, 297, 177

Kriss, G. A., Davidsen, A. F., Zheng, W., Kruk, J. W., & Espey, B. R. 1995, ApJ, 454, L7

Kriss, G. A., et al. 1992, ApJ, 392, 485

Krolik, J. H., & Kriss, G. A. 1995, ApJ, 447, 512

Kruk, J. W., Durrance, S. T., Kriss, G. A., Davidsen, A. F., Blair, W. P., Espey, B. R., & Finley, D. 1995, ApJ, 454, L1

Makishima, K. et al. 1996, PASJ, submitted

Mathur, S., Elvis, M., & Singh, K. P. 1995, ApJ, 455, L9

Mathur, S., Wilkes, B., Elvis, M., & Fiore, F. 1994, ApJ, 434, 493

Mathur, S., Wilkes, B., & Elvis, M. 1995, ApJ, 452, 230

Mushotzky, R. F., Fabian, A. C., Iwasawa, K., Kunieda, H., Matsuoka, M., Nandra, K., & Tanaka, Y. 1995, MNRAS, 272, L9

Nandra, P., & Pounds, K. A. 1994, MNRAS, 268, 405

Netzer, H. 1993, ApJ, 411, 594

Otani, C., et al. 1996, PASJ, in press

Otani, C., et al. 1996, in Röntgensstrahlung from the Universe, eds. Zimmermann, H.U., Trümper, J., & Yorke H. (Garching: MPE) in press

Pogge, R. 1989, ApJ, 345, 730

Reichert, G. A., Mushotzky, R. F., & Holt, S. S. 1986, ApJ, 303, 87

Reynolds, C. S., & Fabian, A. C. 1995, MNRAS, 273, 1167

Schmitt, H. R., & Kinney, A. L. 1996, ApJ, in press

Serlemitsos, P. J., et al., 1995, PASJ, 47, 105

Shafer, R. A., Haberl, F., & Arnaud, K. A. 1989, XSPEC: An X-ray Spectral Fitting Package (ESA TM-09) (Paris: ESA)

Stark, A.A., et al. 1992, ApJS, 79, 77

Tanaka, Y., et al. 1995, Nature, 375, 659

Tanaka, Y., Holt, S.S., & Inoue, H. 1994, PASJ, 46, L37

Tarter, C. B., Tucker, W. H., & Salpeter, E. E. 1969, ApJ, 156, 943

Turner, T.J., Nandra, K., George, I.M., Fabian, A.C., & Pounds, K.A. 1993, ApJ, 419, 127

Ulrich, M.-H., & Boisson, C. 1983, ApJ, 267, 515

Verner, D. A., & Yakovlev, D. G. 1995, A&AS, 109, 125

Voit, G. M., Shull, J. M., & Begelman, M. C. 1985, ApJ, 316, 573

Vrtilek, J. M., & Carleton, N. A. 1985, ApJ, 294, 106

Walter, R., Ulrich, M.-H., Courvoisier, T. J.-L., & Buson, L. M. 1990, A&A, 233, 53

Weymann, R. J., Turnshek, D. A., & Christiansen, W. A. 1985, in Astrophysics of Active Galaxies and Quasi-stellar Objects, ed. J. S. Miller (Mill Valley: University Science Books), 333

Yaqoob, T., Warwick, R. S., & Pounds, K. A. 1989, MNRAS, 236, 153

Yaqoob, T., et al. 1993, MNRAS, 262, 435

Yaqoob, T., Edelson, R., Weaver, K. A., Warwick, R. S., Mushotzky, R. F., Serlemitsos, P. J., & Holt, S. S. 1995, ApJ, 499, L99